J Nanopart Res (2017) 19: 143
DOI 10.1007/s11051-017-3813-y

RESEARCH PAPER

Role of *N*-methyl-2-pyrrolidone for preparation of Fe_3O_4@SiO_2 controlled the shell thickness

Sung-Bok Wee · Hyeon-Cheol Oh · Tae-Gyun Kim · Gye-Seok An · Sung-Churl Choi

Received: 29 December 2016 / Accepted: 1 March 2017 / Published online: 12 April 2017

Abstract We developed a simple and novel approach for the synthesis of Fe_3O_4@SiO_2 nanoparticles with controlled shell thickness, and studied the mechanism. The introduction of *N*-methyl-2-pyrrolidone (NMP) led to trapping of monomer nuclei in single shell and controlled the shell thickness. Fe_3O_4@SiO_2 controlled the shell thickness, showing a high magnetization value (64.47 emu/g). Our results reveal the role and change in the chemical structure of NMP during the core-shell synthesis process. NMP decomposed to 4-aminobutanoic acid in alkaline condition and decreased the hydrolysis rate of the silica coating process.

Keywords Fe_3O_4@SiO_2 · *N*-Methyl-2-pyrrolidone · Binary solvent · Dispersion stability · Shell thickness · Nanocomposites

Introduction

Recent attention in the field of nanoparticles has been focused on Fe_3O_4 nanoparticles due to their unique magnetic properties. These properties make these nanoparticles attractive candidates for ferro-fluids, electronic devices, information storage, and biomedical applications such as an MRI contrasting agent and in DDS and bioseparation (Pankhurst et al. 2003; Safarik and Safarikova 2004; Mornet et al. 2004; Tartaj et al. 2003; Shapiro et al. 2005). In order for Fe_3O_4 to be used in these fields, chemical stability, uniform size distribution, and excellent dispersion properties in suspension are required. However, Fe_3O_4 nanoparticles have shown poor chemical stability and unstable dispersion properties because of the strong anisotropic dipolar attraction between the Fe_3O_4 nanoparticles and the high surface energy of the nanoparticles, which is attributed to a balance between Van der Waals attractive forces and repulsive forces (Zhang et al. 2006; Morel et al. 2008). Due to these properties, Fe_3O_4 nanoparticles easily aggregate, forming large clusters. The agglomerates and large clusters decrease the specific properties of Fe_3O_4 nanoparticles.

There have been many attempts to prevent aggregation and improve the chemical stability and dispersion properties in the suspension of Fe_3O_4 nanoparticles. Physical treatment using ultrasound has been universally applied to improve the dispersion of Fe_3O_4 nanoparticles (Morel et al. 2008; Yang et al. 2005). However, improvements of dispersion properties by physical treatment are not stable, resulting in further agglomeration and precipitation of Fe_3O_4 nanoparticles. In contrast, chemical treatment that enhances steric hindrance or electrostatic repulsion forces results in a suspension with magnetic nanoparticles that is stable for a long time in many liquid media. The addition of a large amount of surfactants in suspension is an efficient chemical

S.-B. Wee · T.-G. Kim · G.-S. An · S.-C. Choi (✉)
Division of Materials Science and Engineering, Hanyang University, 17 Haengdang-dong, Seongdong-gu, Seoul 133-791, South Korea
e-mail: choi0505@hanyang.ac.kr

H.-C. Oh
Korea Nano Plus, Inc., 9-16 Macheon-ro 51gil, Songpa-gu, Seoul, South Korea

treatment approach, and this technique has been heavily researched to improve the chemical stability of the particle surfaces and the dispersion uniformity (Lu et al. 2002; Wee et al. 2016).

Another method to improve the chemical stability and the dispersibility is the addition of a silica coating on the Fe_3O_4 nanoparticles. The silica coating process on the surface of the magnetic nanoparticles may prevent particle aggregation in liquid media and improve the chemical stability. The silanol groups of the silica are easily terminated and can bind with various coupling agents. However, trapping of multiple nuclei in a single silica shell occasionally occurs by agglomerated magnetic nanoparticles prior to or during the silica coating process. A previous report showed that typical distributions of nuclei per shell included mostly monomers, some dimers, and about 10% trimers and greater than trimers. When multiple nuclei were trapped in a single silica shell, degradation in physical and chemical properties was observed (Lu et al. 2002). H. L. Ding et al. (2012) reported that hydrophobic Fe_3O_4 nanoparticles were dispersed and emulsified using Igepal CO-520 (surfactant). They also synthesized Fe_3O_4@SiO_2 nanoparticles using a reverse micro-emulsion method. However, their process composed too many steps and the equivalently fractionated drop method was used (Ding et al. 2012). M. Abbas et al. (2014) studied a method for controlling the silica shell thickness on Fe_3O_4 nanoparticles. However, their process involved a large amount of surfactant and a time-consuming synthesis; thus, their method has a high manufacturing cost, making it difficult to apply in various industrial fields (Abbas et al. 2014).

In order to use Fe_3O_4 nanoparticles in various industrial areas, especially biomedical fields, good dispersion stability and chemical stability are required, and the addition of a large amount of surfactants is severely limited in biomedical applications. However, it is very difficult to disperse Fe_3O_4 nanoparticles with good chemical stability without surfactants because the electrostatic force, steric hindrance effect, and affinity between solvent, particle, and surfactant affect the nanoparticle dispersibility. Herein, we report a method to mass produce Fe_3O_4@SiO_2 nanoparticles without surfactants and an equivalently fractionated drop method that shows good dispersion stability and excellent physicochemical properties. We used binary solvents with various volume ratios between *N*-methyl-2-pyrrolidone (NMP, polar aprotic solvent) and de-ionized water (DIW) to change the electric charge of the particle surface and the silica shell thickness. We also discussed the chemical structure change of NMP during the core-shell synthesis process.

Experimental section

Materials

$FeCl_3 \cdot 6H_2O$ (>97%, Sigma-Aldrich), anhydrous sodium acetate (>98.5%, Samchun Pure Chemical), ethylene glycol (>99.5%, Samchun Pure Chemical), tetraethyl orthosilicate (TEOS, Sigma-Aldrich), ammonia solution (NH_3, Samchun Pure Chemical), ethyl alcohol (EtOH, Samchun Pure Chemical), and NMP (Sigma-Aldrich) were purchased from commercial suppliers and were used as received.

Synthesis

Magnetic nanoparticles

The Fe_3O_4 nanoparticles were prepared according to a polyol method. $FeCl_3 \cdot 6H_2O$ (2.7 g, 0.01 mol), sodium acetate (4.1 g, 0.05 mol), and distilled water (5.4 g, 0.3 mol) were completely dissolved in 100 mL of ethylene glycol via vigorous mechanical stirring. The suspension was heated and refluxed for several hours, during which time the color of the solution turned reddish brown and eventually became black. After cooling to room temperature, the black nanoparticles were magnetically separated by attaching a magnet to the outside of the reaction flask and washing the solution with ethanol and distilled water several times to eliminate organic and inorganic byproducts.

Fe_3O_4@SiO_2 nanoparticles

The Fe_3O_4@SiO_2 nanoparticles were prepared by synthesizing a silica shell using a sol-gel method. Five grams of Fe_3O_4 nanoparticles synthesized using the above method was added to various binary solvents with different solvent volume ratios (total volume 200 mL). The samples were named F@SA, F@SB, F@SC, F@SD, and F@SE. Here, "F@S" indicates Fe_3O_4@SiO_2 nanoparticles, and the letter after the F@S abbreviation indicates the solvent condition during the synthesis process given in Table 1.

The solutions were ultrasonicated for 5 min, and a solution containing 30 mL of TEOS dissolved in 10 mL

Table 1 Abbreviations and solvent conditions for various samples

Abbreviations[a]	Dispersed particles	Solvent (condition)	Initial pH[b]
FA	Synthesized Fe_3O_4	Condition A: H_2O	5.74
FB	Synthesized Fe_3O_4	Condition B: H_2O-NMP (3:1 in volume)	6.36
FC	Synthesized Fe_3O_4	Condition C: H_2O-NMP (1:1 in volume)	7.17
FD	Synthesized Fe_3O_4	Condition D: H_2O-NMP (1:3 in volume)	8.65
FE	Synthesized Fe_3O_4	Condition E: NMP	10.13

[a] Meaning of abbreviations: F = Fe_3O_4, alphabet after F = solvent conditions

[b] The initial pH values when Fe_3O_4 nanoparticles were added in each condition

EtOH was added. After that, 30 mL of an ammonia solution was added to the solution. The total reaction time was 2 h, and the solution was mechanically stirred at room temperature during the reaction. Then, the solution was magnetically separated by attaching a magnet to the outside of the reaction flask. The separated nanoparticles were washed with ethanol and distilled water several times and were then collected.

Characterization

Electrokinetic sonic amplitude (ESA, Zeta Finder, Matec Applied Sciences, USA) was used to analyze the zeta potential value at various pH values in DIW. The pH values of the Fe_3O_4 nanoparticles in DIW were adjusted by the addition of 0.1 M HNO_3 or 0.1 M NaOH.

Analysis of zeta potential values and particle size distribution (Zetasizer Nano ZS, Malvern, UK) was performed to estimate the dispersed particle size distribution and surface charge in a binary solvent. Synthesized Fe_3O_4 was dispersed in various binary solvents, DIW and NMP, and the zeta potential values and pH of that were estimated. The samples were named FA, FB, FC, FD, and FE. The last alphabet means the dispersed solvent conditions given in Table 1. The size and morphology of the nanoparticles were characterized using transmission electron microscopy (TEM, JEM-ARM 200F, JEOL, Japan). Fourier transform infrared (FT-IR) spectroscopy (Nicolet 5700, Thermo Electron, USA) data were also obtained. The magnetic properties and crystallinity of the chemically treated Fe_3O_4 nanoparticles were measured using a vibrating sample magnetometer (VSM, Lake Share 7400, USA) in an external magnetic field ranging from −10 to +10 kOe and X-ray diffraction (XRD, Ultima IV, Rigaku, Japan).

Results and discussion

Figure 1a indicates the variation of the zeta potential values of Fe_3O_4 nanoparticles at different pH values in DIW. The isoelectric point (IEP) of the as-synthesized Fe_3O_4 nanoparticles was determined to be a pH of about 7.0. Zeta potential absolute values of Fe_3O_4 nanoparticles increased in acid or alkaline conditions due to acid-base properties. The surface charge of Fe_3O_4 in acid was changed to positive by H^+ acidity (protonation). The surface charge of Fe_3O_4 in base was modified to negative by OH^- basicity (deprotonation or amphiprotic). It is the acid-base properties (acid-base reaction). The phenomenon increased the absolute value of zeta potential in acid or base condition. However, the absolute values were very weak on a whole range of pH (between −15 and 15 mV), which led to agglomeration of Fe_3O_4 nanoparticles in the suspension. Figure 1b shows the variation in the zeta potential value of Fe_3O_4 dispersed in DIW, NMP, and the binary solvents with different volume ratios. FA, which is the case where DIW was used as solvent, showed a value of +4.28 mV, indicating that the initial dispersion state in DIW was very unstable. However, as the NMP volume ratio in a binary solvent increased, the zeta potential absolute values of Fe_3O_4 nanoparticles were enhanced. Finally, when Fe_3O_4 was dispersed in NMP, the zeta potential value was −66.8 mV (FE). Table 1 shows that the initial pH values of the sample conditions became as the NMP volume ratio in the binary solvent increased (the pH of FE was 10.13). However, even allowing for the alkalinity as the NMP volume ratio increased, the zeta potential value of FE is too high in comparison with that at the same pH value in DIW. The value in DIW is −10 mV at a pH value of 10. NMP induced a negative charge on the surface of the Fe_3O_4 nanoparticles and reduced the surface tension of Fe_3O_4 nanoparticles due to aprotic

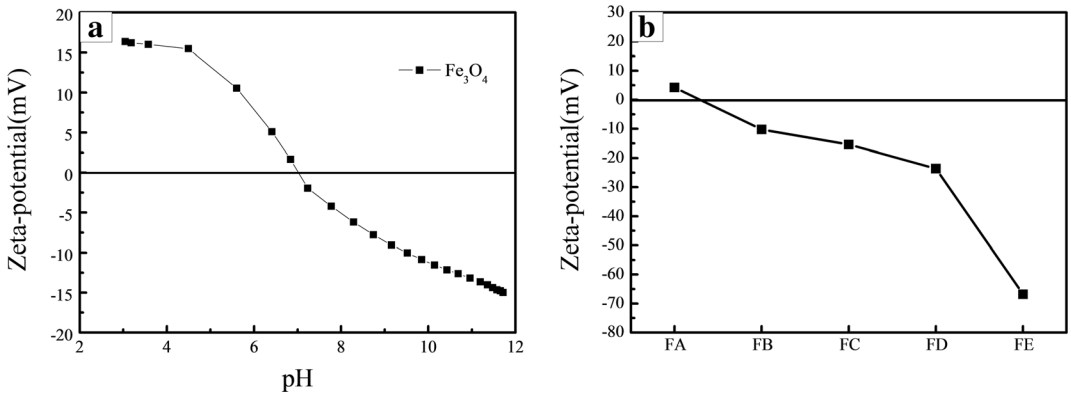

Fig. 1 Zeta potential variation of Fe_3O_4 nanoparticles **a** at different pH values in DIW and **b** in different binary solvents

solvent properties and solvation effect (Lin and Zhang 2012). The aprotic solvent properties and solvation effect of NMP as well as the alkalinity provided the Fe_3O_4 nanoparticles with a high zeta potential value resulting in good dispersibility. The improved initial dispersibility and the alkaline conditions are also advantageous for the preparation of the Fe_3O_4@SiO_2 composite nanoparticles because the growth of the silica layer on the surface of the magnetic cores is usually performed under alkaline conditions, and the dispersibility affects the formation of monomer nuclei (Lu et al. 2002; Philipse et al. 1994). The crystalline structures of the as-synthesized Fe_3O_4 and Fe_3O_4@SiO_2 synthesized in different binary solvents were determined by XRD (Fig. 2). The peaks of Fe_3O_4 and Fe_3O_4@SiO_2 nanoparticles appear in the crystal planes of (220), (311), (400), (422), (511), and (440). These data match well with the JCPDS-International center for Diffraction Data (JCPDS card: 75-1610) for magnetite. An obvious diffraction peak at 25° in the curves of F@SA-F@SE was observed, which is indicative of the amorphous SiO_2 shell on the surface of the Fe_3O_4 nanoparticles. The peak intensities decreased from F@SA to F@SE. This trend may be due to differences in shell thickness. The XRD patterns indicate that Fe_3O_4 cores are very crystalline and the surface functionalization did not change the surface of the Fe_3O_4 phase.

The structural morphology of Fe_3O_4 and Fe_3O_4@SiO_2 nanoparticles was studied by TEM. As shown in Fig. 3, the morphology of the as-synthesized Fe_3O_4 nanoparticles was spherical, and the particles are flocculated. The synthesized Fe_3O_4 nanoparticles were nearly 180 nm in size with a uniform size distribution (Fig. 3a). Figure 3b–f shows TEM images of Fe_3O_4@SiO_2 nanoparticles, which revealed that silica shells were coated on the Fe_3O_4. As the volume ratio of NMP in the binary solvent increased, the silica shell thickness decreased as follows: 115 nm for F@SA, 99 nm for F@SB, 81 nm for F@SC, 36 nm for F@SD, and 10 nm for F@SE. As shown in Fig. 3b, c, Fe_3O_4@SiO_2 nanoparticles were severely aggregated because of the strong attractive force between Fe_3O_4 nanoparticles caused by their high surface energy and low absolute zeta potential values during the synthesis process (Wee et al. 2016). As the NMP content increased in the binary solvent, the flocculation of Fe_3O_4@SiO_2 nanoparticles is decreased (Fig. 3d, e). F@SE was uniformly mono-dispersed and had a uniform size distribution (Fig. 3f).

The particle size distribution and hydrodynamic radius of the synthesized Fe_3O_4@SiO_2 nanoparticles are

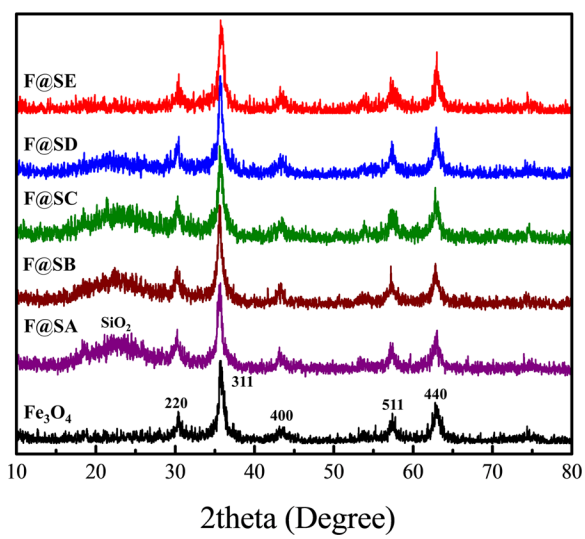

Fig. 2 The XRD pattern of synthesized Fe_3O_4 and Fe_3O_4@SiO_2 nanoparticles synthesized in various binary solvents

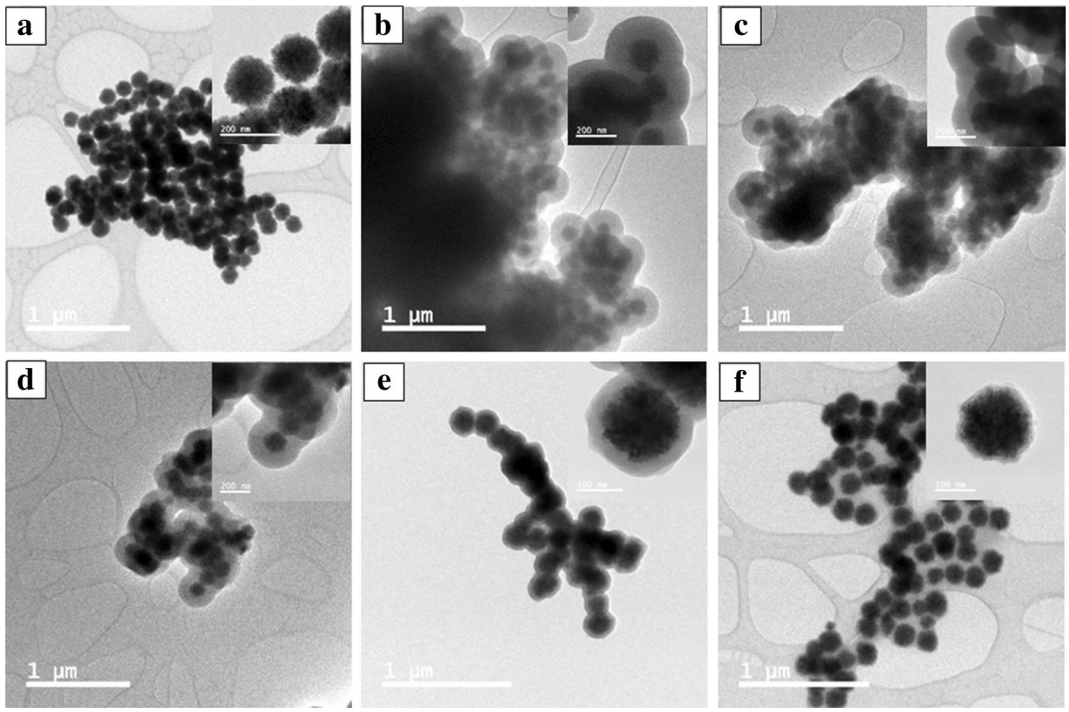

Fig. 3 TEM images of **a** Fe_3O_4 and Fe_3O_4@SiO_2 synthesized in binary solvents with different volume ratios. **b** F@SA. **c** F@SB. **d** F@SC. **e** F@SD. **f** F@SE

shown in Fig. 4 as a function of binary solvent volume ratio. The mean size of F@SA was 1106 nm, and the size distribution was broad due to flocculation and an increase in the hydrodynamic radius by adsorption of molecular H_2O. SiO_2 shell easily absorbs the water molecule. At this time, the whole size distribution peaks become broad by absorbed water molecule. The apparatus of size distribution analysis measured the particle size including absorbed water molecule. The poor dispersity of Fe_3O_4 during the silica coating process led to trapping of multiple nuclei in a single silica shell and very weak surface charge, which caused the flocculation of Fe_3O_4@SiO_2 nanoparticles. The particle size distributions shift to the left in Fig. 4 as the ratio of NMP in the binary solvent increases from F@SB to F@SE. The mean sizes were as follows: 995.4 nm for F@SB, 825 nm for F@SC, and 531.2 nm for F@SD. However, some agglomeration of Fe_3O_4@SiO_2 nanoparticles was still observed for these samples, and their size distribution curves were relatively broad. In contrast, the size distribution curve of F@SE was sharp and the mean size was 220.2 nm, which was very similar to that of the synthesized Fe_3O_4. The particle size distribution and TEM image of F@SE indicates that mono Fe_3O_4 was trapped in single silica shell.

The characteristic bands of the as-synthesized Fe_3O_4 and Fe_3O_4@SiO_2 nanoparticles were obtained through the FT-IR spectra for various binary solvents (Fig. 5). The absorption peak at about 565 cm^{-1} matched the vibration band of the Fe-O functional group, which is a characteristic peak of Fe_3O_4. The Si-OH vibration peak at around 955 cm^{-1} and the Si-O-Si vibration peak at around 1080 cm^{-1} were also observed; these peaks were associated with the SiO_2 shell. As the NMP ratio in

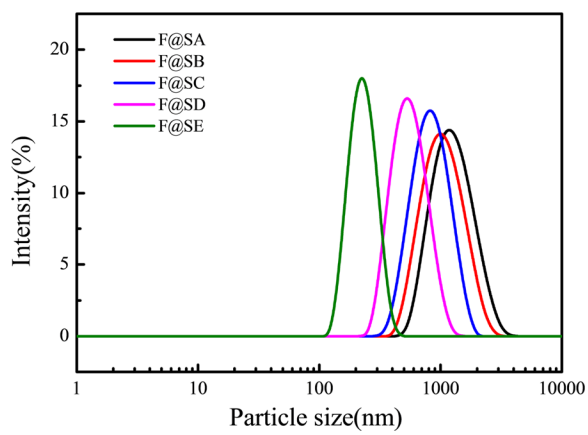

Fig. 4 Particle size distributions of F@SA, F@SB, F@SC, F@SD, and F@SE

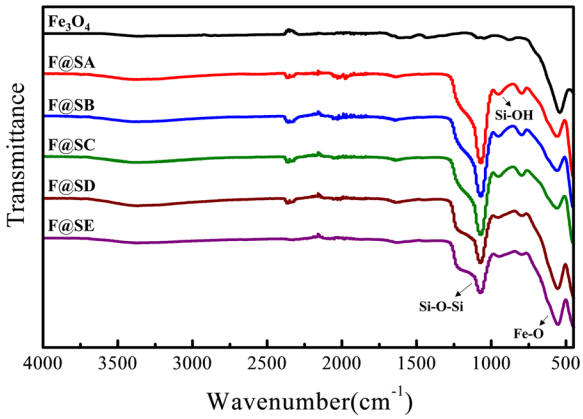

Fig. 5 FT-IR analysis data of Fe_3O_4 and Fe_3O_4@SiO_2 nanoparticles synthesized at various binary solvent conditions

the binary solvent increased, the intensity of the absorption peak related to the silica decreased because the shell thickness decreased. Considering the FT-IR spectra, particle size distribution, and XRD and TEM results, it is clear that the SiO_2 homogeneously coated the Fe_3O_4 surface, and the shell thickness and dispersity were controlled by adjustment of NMP ratio in the binary solvent.

The magnetic hysteresis loops of the prepared Fe_3O_4@SiO_2 nanoparticles are shown in Fig. 6. The saturation magnetization values of Fe_3O_4@SiO_2 were as follows: 36.58 emu/g for F@SA, 39.29 emu/g for F@SB, 42.68 emu/g for F@SC, 54.87 emu/g for F@SD, and 64.47 emu/g for F@SE. The VSM values increased with decreasing nanoparticle shell thickness. The decrease in the saturation magnetization value after coating was attributed to the incorporation of a nonmagnetic silica shell around the core Fe_3O_4 nanoparticles.

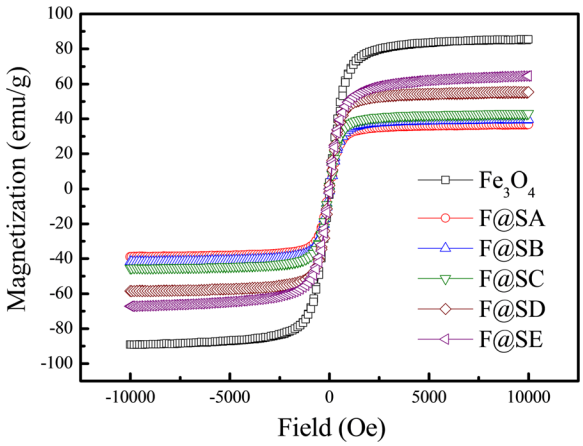

Fig. 6 VSM curves of synthesized Fe_3O_4 and Fe_3O_4@SiO_2 synthesized at various binary solvent conditions

Another possible cause is the formation of chemical bonds between Fe, Si, and O ions resulting from the surface functionalization with SiO_2. When SiO_2 coated the Fe_3O_4, Fe ions at the surface tended to bond with SiO_2, eliminating the magnetic moment of these Fe ions (Dang et al. 2010). Similar decreases in magnetic moment after functionalization with SiO_2 have been reported (Singh et al. 2012; Kolhatkar et al. 2013). Generally, the saturation magnetization values of Fe_3O_4@SiO_2 nanoparticles were less than half of the value of non-coated Fe_3O_4 (85.02 emu/g). In spite of the disadvantage that the silica shells decrease the saturation magnetization values, we achieved a very high magnetization value by controlling the shell thickness (64.47 emu/g for F@SE).

Figure 7 shows the relationship between the zeta potential values and the silica shell thickness of Fe_3O_4@SiO_2 nanoparticles for different volume ratios of the binary solvent. As the NMP ratio in the binary solvent increased during the coating process, the silica shell thickness decreased from around 115 to 10 nm (red circle in Fig. 5), and the corresponding zeta potential values were −90.1 to −56.8 mV. The surface charge of Fe_3O_4@SiO_2 was affected by the amount of whole SiO_2 shell (Jang 2012). Consequently, the technique using binary solvents provided very high zeta potential values of Fe_3O_4@SiO_2 nanoparticles in spite of very thin SiO_2 shell thickness.

Figure 8 illustrates an explanation of the structure change of NMP during the core-shell synthesis process. The structure change of NMP to pyrrolidone chemical structure mixed in DIW was a general phenomenon. We supposed that NMP could change to 4-aminobutanoic acid directly or via a pyrrolidone chemical structure under strong alkaline conditions by added NH_4OH

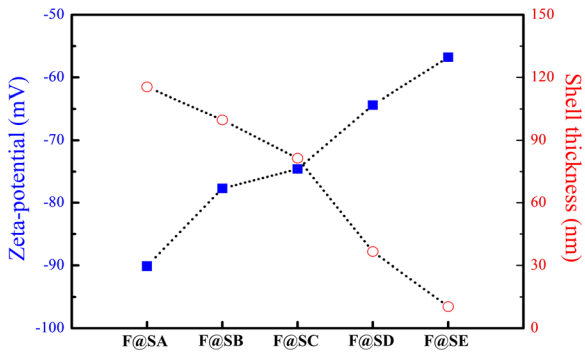

Fig. 7 The relationship between zeta potential values, binary solvent volume ratios, and silica shell thickness

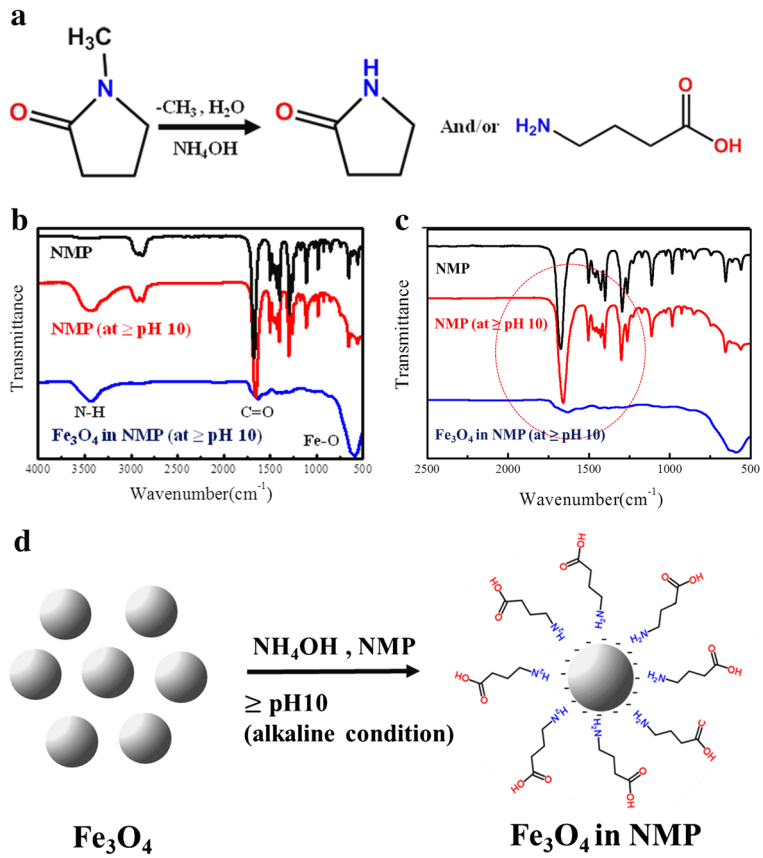

Fig. 8 **a** NMP decomposition mechanism. **b** FT-IR analysis data of NMP and Fe_3O_4 in NMP. **c** The magnified data of C=O peak in **b**. **d** The role of NMP near Fe_3O_4 nanoparticles

(Fig. 8a). As shown Fig. 8b, the black line is the FT-IR spectroscopy result of pure NMP, the red line is that of NMP with NH_4OH, and the blue line is that of Fe_3O_4 particles dispersed in NMP with NH_4OH. FT-IR spectroscopy results indirectly show the present of 4-aminobutanoic acid. Firstly, N-H peak was not observed in pure NMP, while it was appeared in NMP with NH_4OH. It revealed that NMP with NH_4OH decomposed to 4-aminobutanoic acid or pyrrolidone chemical structure. Secondly, the presence of C=O of Fe_3O_4 particles dispersed in NMP with NH_4OH (blue line) revealed the existence of carboxyl group on Fe_3O_4 surface. Because there is no additive without NMP, NH_4OH, and Fe_3O_4 nanoparticles, the source of C=O peak on Fe_3O_4 is attributed to NMP combined with Fe_3O_4. In order to combine with Fe_3O_4, the pentagonal molecular structures of NMP may be cut off. Fe_3O_4 nanoparticles have a negative charge under alkaline conditions. Thirdly, the C=O peak shifts to right in Fig. 8c (black line 1681 cm^{-1}, red line 1652 cm^{-1}, blue line 1633 cm^{-1}). The C=O peak of pyrrolidone ring is in 1750~1650 cm^{-1}, and the peak of carboxyl group is in 1650–1550 cm^{-1}. It is strong evidence that the pyrrolidone ring was decomposed. As a result, the amine functional groups of 4-aminobutanoic acid moved to the nanoparticle surface and were bonded by electrical attraction. This resulted in the carboxyl group of 4-aminobutanoic acid facing the solvent (Fig. 8d), which induced a negative surface charge that improved the dispersion due to electrostatic forces and solvation effects. Furthermore, NMP acts as a surfactant under strong alkaline conditions due to increased steric hindrance effect and affinity by change of NMP chemical structure and solvation effect (Lin and Zhang 2012).

The enhanced electrostatic repulsion force and reduced surface tension with increased NMP in the binary solvent improved the dispersibility of Fe_3O_4 nanoparticles during the silica coating process. Furthermore, NMP decreased the hydrolysis rate of the silica coating process due to a deprotonation reaction. As a result, the NMP ratio in the binary solvent was used to control the hydrolysis rate, which resulted in a decreased shell thickness (Rao et al. 1999). Consequently, a combination of the salvation effect, aprotic properties, and

alkalinity of NMP improved the dispersity of nanoparticles and monomer trapping phenomenon in single silica shell as well as controlled the shell thickness by adjusting the hydrolysis rate.

Conclusions

In conclusion, we have demonstrated a simple and novel approach for the synthesis of Fe_3O_4@SiO_2 nanoparticles via a novel sol-gel method without surfactants. We functionalized Fe_3O_4 nanoparticles with uniform silica shells using NMP, and we controlled SiO_2 shell thickness by a novel and simple method. Fourier transform infrared (FT-IR) analysis revealed the structure change of NMP under strong alkaline conditions. NMP also decreased the hydrolysis rate of the silica coating process due to a deprotonation reaction, which resulted in a decreased shell thickness. Fe_3O_4@SiO_2 nanoparticles were homogeneously synthesized with trapping of monomer nuclei in single silica shell and excellent magnetization values (64.47 emu/g). Our results provide not only the novel sol-gel method to mass produce Fe_3O_4@SiO_2 nanoparticles with excellent magnetization value, but also the role of NMP that can be applied to disperse and synthesize other core-shell nanoparticles.

Acknowledgments The work presented in this paper was supported by a National Research Foundation of Korea (NRF) grant funded by the Ministry of Science, ICT & Future Planning Science and Technology (2014R1A2A1A11050220).

Compliance with ethical standards

Conflict of interest Authors S.B. Wee, T.G. Kim, and G.S. An have received research grants from the National Research Foundation of Korea (NRF).

References

Abbas M, Torati SR, Lee CS, Rinaldi C, Kim CG (2014) Fe_3O_4/SiO_2 core/shell nanocubes: novel coating approach with tunable silica thickness and enhancement in stability and biocompatibility. J Nanomed Nanotechnol 5:244

Dang F, Enomoto N, Hojo J, Enpuku K (2010) Sonochemical coating of magnetite nanoparticles with silica. Ultrason Sonochem 17:193–199

Ding HL, Zhang YX, Wang S, Xu JM, Xu SC, Li GH (2012) Fe_3O_4@SiO_2 core/shell nanoparticles: the silica coating regulations with a single core for different core sizes and shell thicknesses. Chem Mater 24:4572–4580

Jang ES (2012) Preparation of Fe_3O_4/SiO_2 core/shell nanoparticles with ultrathin silica layer. Korean Chem Soc 56:478–483

Kolhatkar AG, Jamison AC, Litvinov D, Willson RC, Lee TR (2013) Tuning the magnetic properties of nanoparticles. Int J Mol Sci 14:15977–16009

Lin L, Zhang S (2012) Effective solvothermal deoxidization of graphene oxide using solid sulphur as a reducing agent. J Mater Chem 22:14385–14393

Lu Y, Yin Y, Mayers BT, Xia Y (2002) Modifying the surface properties of superparamagnetic iron oxide nanoparticles through a sol−gel approach. Nano Lett 2:183–186

Morel AL, Nikitenko SI et al (2008) Sonochemical approach to the synthesis of Fe_3O_4@SiO_2 core−shell nanoparticles with tunable properties. ACS Nano 2:847–856

Mornet S, Vasseur S, Grasset F, Duguet E (2004) Magnetic nanoparticle design for medical diagnosis and therapy. J Mater Chem 14:2161–2175

Pankhurst QA, Connolly J, Jones SK, Dobson J (2003) Applications of magnetic nanoparticles in biomedicine. J D: Appl Phys 36:R167–R181

Philipse AP, MPB v-B, Pathmamanoharan C (1994) Magnetic silica dispersions: preparation and stability of surface-modified silica particles with a magnetic core. Langmuir 10:92–99

Rao AV, Sakhare HM, Tamhankar AK, Shinde ML, Gadave DB, Wagh PB (1999) Influence of N,N-dimethylformamide additive on the physical properties of citric acid catalyzed TEOS silica aerogels. Mater Chem Phys 60:268–273

Safarik I, Safarikova M (2004) Magnetic techniques for the isolation and purification of proteins and peptides. BioMag Res Techn 7:1

Shapiro E, Skrtic S, Koretsky AP (2005) Sizing it up: cellular MRI using micron-sized iron oxide particles. Magn Reson Med 53:329–338

Singh RK, Kim TH, Patel KD, Knowles JC, Kim HW (2012) Biocompatible magnetite nanoparticles with varying silica-coating layer for use in biomedicine: physicochemical and magnetic properties, and cellular compatibility. J Biomed Mater Res Part A 100A:1734–1742

Tartaj P, Morales MP et al (2003) The preparation of magnetic nanoparticles for applications in biomedicine. Phys D: Appl Phys 36:R182–R197

Wee SB, An GS, Han JS, Oh HC, Choi SC (2016) Co-dispersion behavior and interactions of nano-ZrB_2 and nano-SiC in a non-aqueous solvent. Ceram Int 42:4658–4662

Yang C, Wang G, Lu Z, Sun J, Yang W, Zhuang J (2005) Effect of ultrasonic treatment on dispersibility of Fe_3O_4 nanoparticles and synthesis of multi-core Fe_3O_4/SiO_2 core/shell nanoparticles. J Mater Chem 15:4252–4257

Zhang L, He R, Gu HC (2006) Oleic acid coating on the monodisperse magnetite nanoparticles. Appl Surf Sci 253:2611–2617